Solid-State Electronics Vol. 36, No. 12, pp. 1697–1709, 1993
Printed in Great Britain.

0038-1101/93 $6.00 + 0.00

TRANSPORT VIA THE LIOUVILLE EQUATION AND MOMENTS OF QUANTUM DISTRIBUTION FUNCTIONS

H. L. GRUBIN†, T. R. GOVINDAN† and J. P. KRESKOVSKY†
Scientific Research Associates, P.O. Box 1058, Glastonbury, CT 06033, U.S.A.

M. A. STROSCIO
Army Research Office, Research Triangle Park, NC 27709-2211, U.S.A.

(Received 7 February 1993; in revised form 6 May 1993)

Abstract—This paper (i) examines through numerical solutions of the coupled *coordinate representation* Liouville and Poisson equations, the use of the Bohm quantum potential to represent the equilibrium distribution of density and energy in quantum feature size structures; (ii) discusses the development of the nonequilibrium quantum hydrodynamic (QHD) equations with dissipation through the truncation of the quantum distribution function; and (iii) compares select results of the QHD equations incorporating the Bohm potential to the exact Liouville equation solutions. The broad conclusion of the study is that for structures of current interest such as HEMTs, only quantum mechanical solutions, or the incorporation of the quantum potential as a modification of the classical equations will permit representative solutions of such critical features as the sheet charge density.

INTRODUCTION

Advances in crystal growth and processing techniques have assured the construction of nanoscale devices with sharp interfaces. Concomitantly, new device concepts have emerged, including resonant tunneling structures, quantum wires, quantum dots; and varients of classical structures with quantum features, e.g. HEMTs and HBTs. While all devices are governed by quantum mechanics, many devices including HEMTs and HBTs do not require quantum transport for a description of their basic operation. Nevertheless, quantum mechanics is required to provide key electrical features. For example, HBTs sustain low levels of current at low bias levels; these currents are dominantly tunneling currents. Thermionic contributions to current occur at high bias levels. Recently, device formulations utilizing the drift and diffusion equations and the moments of the Boltzmann transport equation were generalized to include a description of tunneling currents (Ancona and Iafrate[1], Grubin and Kreskovsky[2]). These newer studies indicated that quantum contributions of the type first considered by Wigner[3], could be incorporated as modifications to the more traditional approaches to studying transport of carriers through devices. Such an approach was taken by Zhou and Ferry[4,5] in a study of quantum contributions to transport in MESFETs. How well do the quantum modifications of classical transport represent actual transport? This question is addressed for a limited number of cases through comparison of (i) quantum "corrected" solutions with (ii) exact *coordinate representation* solutions to the quantum Liouville equation for the density operator ρ_{op}, whose time dependence is governed by the Hamiltonian H:

$$i\hbar\partial\rho_{op}/\partial t = [H, \rho_{op}]. \quad (1)$$

The relevant quantity in the Liouville simulations is the density matrix $\rho(\mathbf{x}, \mathbf{x}', t) = \langle \mathbf{x}|\rho_{op}|\mathbf{x}'\rangle$ whose role is similar to that of the distribution function in classical physics.

The procedure for assessing the quantum contributions has two parts: *First*, approximate and exact equilibrium solutions to the dissipationless quantum Liouville equation for a variety of structures, including a barrier, are compared. The approximate solutions which arise from a new procedure, with results similar to that of Wigner[3], are also expressed in terms of the Bohm quantum potential[6]:

$$Q_B \equiv -(\hbar^2/2m)[d^2(\rho)^{1/2}/dx^2]/(\rho)^{1/2}, \quad (2)$$

whose physical significance is addressed. *Second*, the quantum Liouville equation with Fokker–Planck dissipation mechanisms is introduced[7]; from which a new derivation of the quantum hydrodynamic (QHD) equations are obtained. Nonequilibrium zero current QHD and exact Liouville solutions are compared for a simple heterostructure diode configuration relevant to HEMT structures. We confirm that the simplest version of the QHD equations, the drift and diffusion current density equation, and its zero current solution are modified as follows[1,2]:

$$J(x, t) = \rho\mu k_b T\partial[(V + aQ_B)/k_b T + \ln(\rho)]/\partial x \quad (3)$$

$$\rho = \rho_0 \exp - [V(x) + aQ_B(x)]/k_b T, \quad (4)$$

†Supported by AFOSR, ARO and ONR.

where a is a constant, determined analytically below and in [1] to be $a = 1/3$. More often a is chosen to provide the best fit to exact results, and is thus determined from numerical simulations as discussed below. Any value of a other than $a = 1$ is of concern, in that arguments associated with the single particle Schrodinger equation, suggest a value of unity, see e.g. [2]. Nevertheless, we show for conditions appropriate to Boltzmann statistics, that the exact and approximate solutions for $a \neq 1$ are remarkably similar; and that solutions without quantum contributions will not represent the local charge distribution in barrier dominated structures. Finally, the results are related to earlier work on the Wigner function for mixed and pure states[8]. These latter issues are addressed in the appendices, which also include a discussion of the numerical algorithm.

THE EXACT EQUATION OF MOTION FOR THE DENSITY MATRIX

The Liouville equation in the coordinate representation without dissipation is:

$$\partial\rho/\partial t + (\hbar/2mi)(\nabla_x^2 - \nabla_{x'}^2)\rho - (1/i\hbar)[V(\mathbf{X}, t) - V(\mathbf{X}', t)]\rho = 0. \quad (5)$$

Solutions yield the time dependent density matrix $\rho(\mathbf{X}, \mathbf{X}', t)$, whose diagonal components provide the density, and whose values are constrained by the integral: $\int d^3\mathbf{X}\rho(\mathbf{X}, \mathbf{X}) = N_0$, where N_0 is the total number of electrons. Assuming free particle conditions along the Y and Z directions, the density matrix, with $\lambda^2 = \hbar^2/2mk_bT$, separates and we seek $\rho(X, X', t)$:

$$\rho(\mathbf{X}, \mathbf{X}', t) = \rho(X, X', t) \times \exp - [\{(Y - Y')^2 + (Z - Z')^2\}/4\lambda^2]. \quad (6)$$

Here λ, is the thermal de Broglie wavelength. Equation (5) separates and the X, X' portion is rewritten in terms of center of mass and nonlocal coordinates:

$$\text{center of mass coordinates: } (X + X')/2 = x;$$
$$\text{nonlocal coordinates: } (X - X')/2 = \zeta. \quad (7)$$

Note: the transformation is consistent with [3], but is not area preserving (the Jacobian is not unity). In terms of these variables and for free particle conditions along the other directions, the governing equation for $\rho(x + \zeta, x - \zeta, t)$ is:

$$\partial\rho/\partial t + (\hbar/2mi)\partial^2\rho/\partial x\partial\zeta - (1/i\hbar)[V(x + \zeta, t) - V(x - \zeta, t)]\rho = 0. \quad (8)$$

All results arise from $\rho(x + \zeta, x - \zeta)$; nevertheless, we require expressions for current and energy, which are obtained from the diagonal components of the following matrices:

$$\text{density: } \rho(x + \zeta, x - \zeta); \quad (9a)$$

$$\text{current density: } j(x + \zeta, x - \zeta) = [\hbar/(2mi)]\partial\rho/\partial\zeta; \quad (9b)$$

$$\text{energy density: } E(x + \zeta, x - \zeta) = -(\hbar^2/8m)\partial^2\rho/\partial\zeta^2. \quad (9c)$$

The above definitions are discussed in [7], and in Appendix B.

THE APPROXIMATE DENSITY MATRIX EQUATION AND EQUILIBRIUM SOLUTION

Numerical solutions are obtained from eqn (8). For interpretive purposes and for developing the QHD equations, we approximate eqn (8) in two steps. *First*, we assume an infinitely differentiable potential, in which case eqn (8) becomes:

$$\partial\rho/\partial t + (\hbar/2mi)\partial^2\rho/\partial x\partial\zeta - (2/i\hbar) \times \sum[1/(2l + 1)!]\zeta^{(2l+1)}\partial^{(2l+1)}V/\partial x^{(2l+1)}\rho = 0, \quad (10)$$

where the sum is over $0 \leqslant l < \infty$. *Second*, we retain only the first two terms in the expansion:

$$\partial\rho/\partial t + (\hbar/2mi)\partial^2\rho/\partial x\partial\zeta - (1/i\hbar)[2\zeta\partial V/\partial x + (\zeta^3/3)\partial^3 V/\partial x^3]\rho = 0. \quad (11)$$

Note: retaining only the term linear in ζ, yields an equation equivalent to the time dependent collisionless Boltzmann equation; demonstrating that quantum effects arise from higher order terms in the expansion of $[V(x + \zeta, t) - V(x - \zeta, t)]$. For the density matrix equivalent to the collisionless Boltzmann equation, and for $\partial\rho/\partial t = 0$:

$$\rho(x + \zeta, x - \zeta, t) = \rho_0 \exp - [\zeta^2/\lambda^2 + \beta V(x)] \quad (12)$$

is an exact solution for free particles (no collisions) in a potential energy distribution $V(x)$. More generally: $\rho(\mathbf{X}, \mathbf{X}', t) = \rho_0 \exp - [\zeta^2/\lambda^2 + \beta V(x)]\exp - [\{(Y - Y')^2 + (Z - Z')^2\}/4\lambda^2]$. For a reference density ρ_0, *the Fermi energy* $E_F = [1/\beta]\ln[\rho_0/\mathbf{N}]$, where $\mathbf{N} = 2(m/2\pi\beta\hbar^2)^{3/2}$. Equation (12) is equivalent to $\exp[-\beta\{(p^2/2m) + V(x)\}]$ (see Appendix B).

To obtain the quantum modifications, we recognize that the classical carrier density and mean kinetic energy density under zero current conditions are respectively: $\rho(x, x) = \rho_0 \exp - [\beta V(x)]$, and $E(x, x) \equiv \epsilon(x, x)\rho(x, x) = \rho(x, x)k_bT/2$, where $\epsilon(x, x)$ is the *mean kinetic energy per particle*, and that eqn (12) can be recast as:

$$\rho(x + \zeta, x - \zeta) = \rho(x, x)\exp - [2\zeta^2\beta\epsilon(x, x)/\lambda^2]. \quad (13)$$

Equations (13) and (12) have the same content for classical transport. For quantum transport the mean kinetic energy per particle includes modifications to the classical value[3]. The numerical studies below suggest that the effect of the quantum correction is to either *pinch* or *stretch* the density matrix along the nonlocal direction. Equation (13) represents both contributions. To obtain these corrections eqn (13) is

substituted into eqn (11) with the resulting equation ordered in powers of ζ:

$$\zeta\{4\partial[\epsilon(x,x)\rho(x,x)]/\partial x + 2(\partial V/\partial x)\rho(x,x)\} - (8\zeta^3/\lambda^2)\{(\beta\epsilon(x,x)\partial\epsilon(x,x)/\partial x - (\lambda^2/24)\partial^3 V/\partial x^3)\rho(x,x)\} = 0. \quad (14)$$

Thus separately:

$$2\partial[\epsilon(x,x)\rho(x,x)]/\partial x + (\partial V/\partial x)\rho(x,x) = 0 \quad (15)$$

$$\epsilon(x,x)\partial\epsilon(x,x)/\partial x - (\lambda^2/24\beta)\partial^3 V/\partial x^3 = 0. \quad (16)$$

Equation (16) submits to an immediate solution: $\epsilon(x,x) = \epsilon_0[1 + (\lambda/\epsilon_0)^2(1/12\beta)\partial^2 V/\partial x^2]^{1/2}$, where $\epsilon_0 = k_b T/2$ is independent of position and the integration constant is chosen to retrieve the classical result under uniform field and density conditions. If the quantum corrections are small compared to ϵ_0, the quantum corrected energy is:

$$E(x,x) \equiv \epsilon(x,x)\rho(x,x) = [k_b T/2 + (\lambda^2/12)\partial^2 V/\partial x^2]\rho(x,x), \quad (17)$$

which corresponds to Wigner's result ([3], eqn (30)). For the quantum corrected density, we solve a rearranged eqn (15), using eqn (17) for energy:

$$[(\lambda^2/6)(\partial^3 V/\partial x^3) + \partial V/\partial x] / [(\lambda^2/6)(\partial^2 V/\partial x^2) + 1/\beta] + \partial \ln \rho/\partial x = 0. \quad (18)$$

For small quantum modifications the above integrates (approximately) to:

$$\rho(x,x) = \rho_0[\exp -\beta(V + Q_W/3)], \quad (19)$$

where:

$$Q_W = (\hbar^2/4m)\beta[\partial^2 V/\partial x^2 - \beta(\partial V/\partial x)^2/2] \quad (20)$$

defines a Wigner quantum potential. *For small* modifications eqn (19) becomes: $\rho(x,x) \approx \rho_0[\exp -\beta V(x)]\{1 - \beta Q_W/3\}$, which corresponds to Wigner's equation (28).

Equations (19) and (4) have the same form although the modification is in terms of potential energy rather than density. To the extent that the above approximations are of order $\hbar^2$, we replace the potential energy in eqn (20) with its classical density equivalent: $\beta V(x) = -\ln[\rho(x,x)/\rho_0]$. In this case $Q_B = Q_W$, and eqn (4) is retrieved with $a = \frac{1}{3}$. In terms of density, the energy [eqn (17)] is reexpressed as:

$$E(x,x) = [k_b T/2 - (\hbar^2/24m)\partial^2(\ln \rho)/\partial^2 x]\rho(x,x). \quad (21)$$

The quantum corrected form of the density matrix using eqns (13), (17) and (19) is:

$$\rho(x+\zeta, x-\zeta) = \rho_0 \exp -[\beta\{V(x) + Q_W/3\} + (\zeta/\lambda)^2\{1 + (\lambda^2/6)\beta\partial^2 V/\partial x^2\}]. \quad (22)$$

For small corrections, $\rho(x+\zeta, x-\zeta) \simeq \rho_0 \exp -[(\zeta/\lambda)^2 + \beta V(x)]\{1 - \beta Q_W/3 - (\zeta^2/6)\beta\partial^2 V/\partial x^2\}$, which as discussed in Appendix B, yields upon application of the Weyl integral, Wigner's form of the quantum corrections (eqn (25) of [3]).

Equation (19) highlights the quantum modifications. For example, in the case of a symmetric barrier, classical theory teaches that density is determined solely by the value of the potential. Quantum theory is predicated upon continuity of the wave functions, permits tunneling, and teaches that the density within a barrier can be higher than that determined classically. At the peak of the barrier, $V_x = 0$, $V_{xx} < 0$, $Q_W < 0$ and the density exceeds its classical value. Within a symmetric quantum well, at the center of symmetry, $V_x = 0$, $V_{xx} > 0$, $Q_W > 0$ and the density can be less than that obtained classically.

COMPARISON OF EXACT AND APPROXIMATE EQUILIBRIUM DISTRIBUTION FUNCTIONS

The extent to which quantum modification represent quantum transport in structures under equilibrium was addressed in two steps. *First*, solutions were obtained for the coupled Liouville equation (8) and Poisson's equation:

$$\partial[\epsilon(x)\partial V/\partial x]/\partial x = -e^2[\rho(x,x) - \rho_D(x)]. \quad (23)$$

(In the discussion below, the permittivity and effective mass are constant, with values are those appropriate to GaAs.) *Second*, the *exact* density computed from the Liouville equation was inserted into eqn (2), Q_B was computed, and an *approximate density* and energy per particle was obtained. The results of part *one* and part *two* were compared. In all calculations global charge neutrality occured: $\int dx[\rho(x,x) - \rho_D(x)] = 0$. Two examples were considered, each at 300 K, where for GaAs the thermal de Broglie wavelength is $\lambda = 45$ Å. In both calculations the nominal density was $10^{18}/cm^3$. (At these densities gallium arsenide calculations necessitate the use of Fermi statistics. These have been performed by the authors[10], and demonstrate *two* density dependent contributions to energy, one classical and a second quantum mechanical in origin. At lower densities where Fermi statistics are not an issue calculations demonstrate that the effects of the quantum potential Q_B are qualitatively similar to the results discussed below, but the magnitudes of the density derivatives are smaller (longer Debye length) and the quantum corrections are reduced.)

Classical $N^+N^-N^+$ structures

The structure is 1600 Å long with a nominal doping of $10^{18}/cm^3$ and a centrally placed 500 Å, $10^{15}/cm^3$ region. The variation in background doping was over one grid point or 4 Å. Solutions yield $\rho(X, X')$, which in equilibrium is real and symmetric, $\rho(X, X') = \rho(X', X)$, as displayed in Fig. 1(a). The inset to Fig. 1(a) is the free particle density matrix. *Free particle Boltzmann boundary conditions* are assumed; i.e. $\rho(X, X') = \rho_0 \exp -(\zeta/\lambda)^2$. All numerical

calculations are compared to eqn (4) for the approximate density and the following for the approximate energy per particle [where a is has the same significance as that in eqn (4)]:

$$\epsilon(x, x) = k_b T/2[1 - (a\lambda^2/2)\partial^2(\ln \rho)/\partial x^2]. \quad (24)$$

The density $\rho(x) \equiv \rho(x, x)$, is represented by the line plot in Fig. 1(b); as is the density obtained from the eqn (4), where $a = 1/3$. The density is ostensibly classical; the quantum corrected density, represented by the dashed lines, closely follows the exact solution. The self consistent potential energy $V(x)$ is displayed in Fig. 1(c), and shows an increase across the N^- region, which accompanies a decrease in charge density across this same region. We are also dealing with a tunneling problem, particularly with those carriers whose energy is below the potential barrier, which in this case has a height of approx. 75 meV. Note: the mean energy of the entering carriers is $k_b T/2 < 75$ meV.

The quantum potential is shown in Fig. 1(d). At the boundary regions $Q_B = 0$; at or near the interface regions Q_B is alternatively positive and negative, and reflects changes in the curvature of the potential. The magnitude of Q_B is approx. 3–5 meV and is nearly 30% of the mean energy of the entering carriers, as given by $k_b T/2$. The signs of Q_B are consistent with continuity of the wavefunction and its derivative through the potential energy barrier region, and weakly prevent the density from approaching its classical value outside (within) the barrier, which instead assumes a smaller (larger) value. This decreased value of density outside the barrier has been described as arising from quantum "repulsion"[11]. The mean energy per particle is displayed in Fig. 1(e), where the solid line represents the exact solution to the Liouville equation [obtained from the ratio of the diagonal components of eqns (9a) and (9c)]. The dashed lines represent eqn (24) for energy, with different values of the coefficient a. The results closest

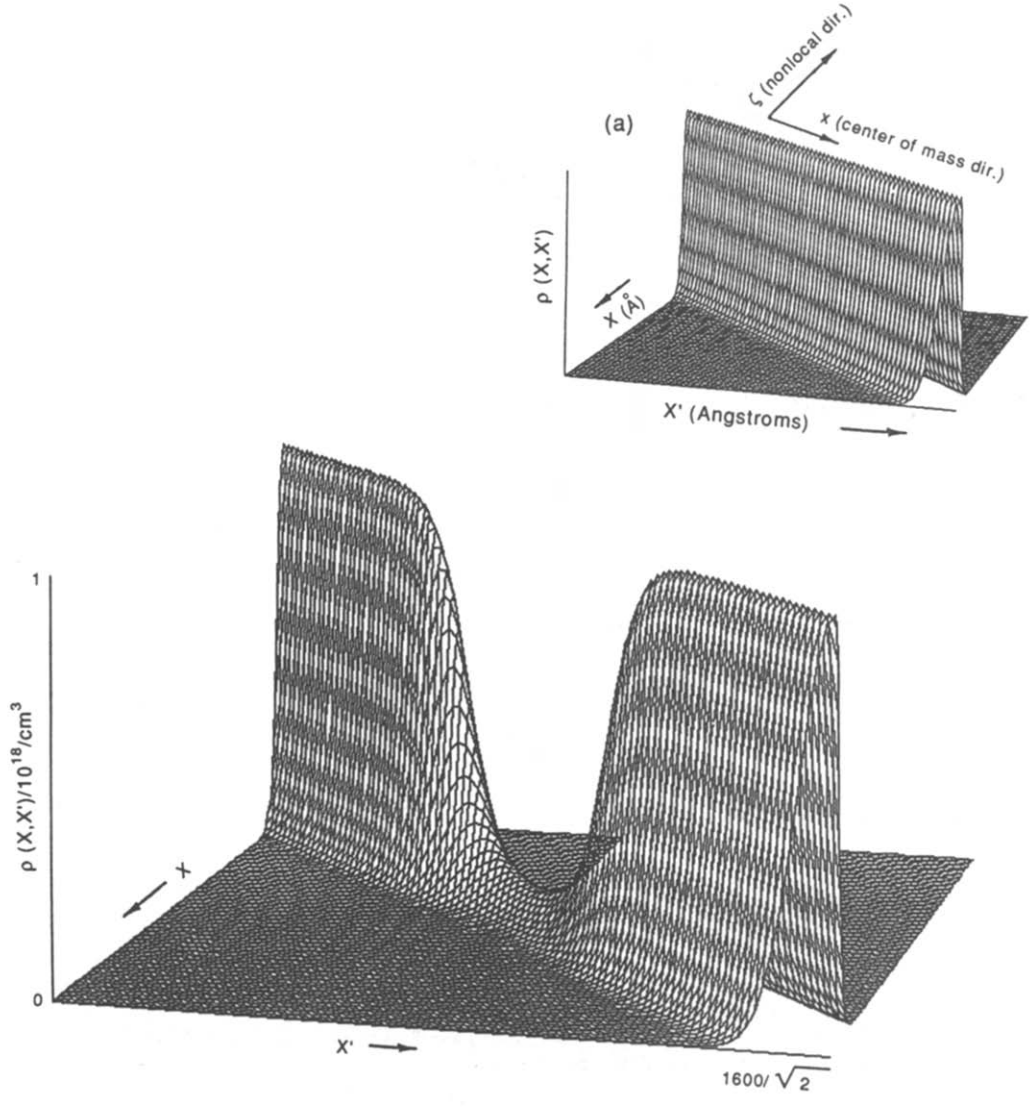

Fig. 1(a). *Caption on facing page.*

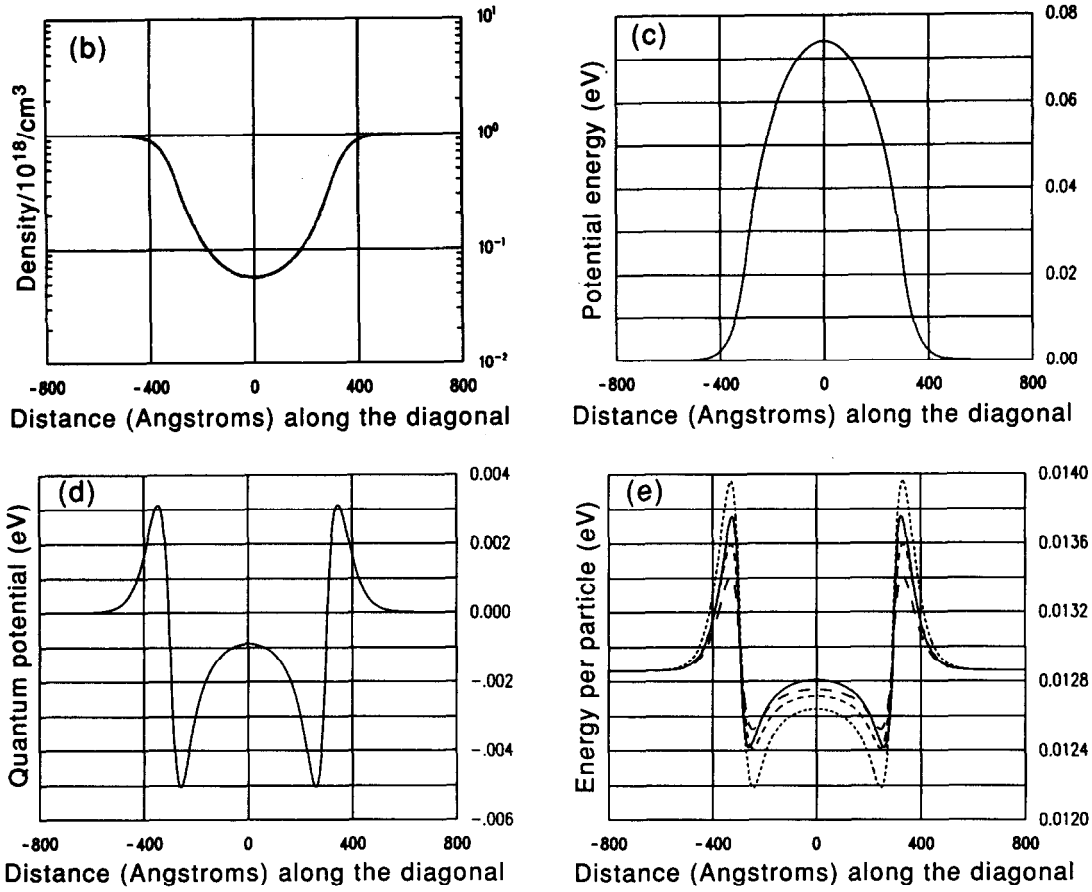

Fig. 1. (a) Density matrix for the $N^+N^-N^+$ structure with free particle boundary conditions, as obtained from the Liouville equation (8). The physical dimension of the structure is 1600 Å, requiring that the density matrix, which is calculated over a square matrix, is of side $1600\,\text{Å}/\sqrt{2}$. The center of mass and nonlocal coordinates are indicated. The inset is the free particle density matrix. (b) (——) Diagonal component of the density matrix from (a). (---) Density as obtained from eqn (4) with $a = 0$; (– – –) with $a = 1/3$. (c) Self consistent potential energy for the calculation of (a). (d) Quantum potential for the calculation of (a). (e) (——) Energy per particle as obtained from the diagonal component of eqn (9c) for the calculation of (a). (— —) Energy per particle as obtained from eqn (24) with $a = 1/3$; (– – –) with $a = 1/4$; (---) with $a = 1/5$.

to the exact solution occur for a between 1/3 and 1/4. The significance of these results is that the quantum contributions are solely responsible for the spatial variation in the energy per particle, and demonstrates the presence of quantum contributions with classical structures.

Single barrier diodes

For this calculation the background density is flat and equal to $10^{18}/\text{cm}^3$; the structure is 2000 Å long and the grid spacing is uniform and equal to 3.33 Å. Figure 2 displays the results for a 500 meV barrier represented analytically by:

$$V_{\text{barrier}}(x) = 500\,\text{meV}[\{1 + \tanh[(x - a_1)/b]\}/2 + \{1 - \tanh[(x - a_2)/b]\}/2 - 1], \quad (25)$$

where $a_1 = -150$ Å, $a_2 = 150$ Å, $b = 50$ Å/3.80. Figure 2(a) displays eqn (25), where V_{barrier} increases continuously (from near zero) to 500 meV, over approx. 75 Å.

Figure 2(b) displays $\rho(X, X')$. As in the Fig. 1 calculation, free particle boundary conditions are assumed. The dramatic "hole" is a consequence of the barrier. Figure 2(c) is a line plot of density. The solid line is obtained from the Liouville and Poisson equations; the dashed lines are from eqn (4) with $a = 0$ (long dashed line) and 1/3 (short dashed line). Common to each calculation is a significant reduction of charge within the barrier, as well as charge accumulation on either side of the barrier. At the edges of the barrier the solutions closest to the Liouville equation are those for $a = 1/3$. The reduction of charge within the barrier is a consequence of the barrier, while the presence of charge adjacent to but outside of the barrier is a consequence of self-consistency in the calculation. Its magnitude is dependent on the condition of global charge neutrality. Figure 2(d) displays the potential energy

distribution. The lowering of the potential adjacent to but outside of the barrier (approx. 65 meV) is a consequence of the excess charge and self-consistency. It is important to recognize that the difference between the peak voltage and the minimum voltage is approx. 380 meV which is less than the 500 meV maximum value of the barrier. This lower value is a consequence of the gradual increase in potential from its minimum value. For an abrupt heterostructure, later calculations demonstrate that all of the offset voltage falls at the interface.

Q_B is displayed in Fig. 2(e). Of significance here is the positive (negative) value of Q_B outside (inside), but adjacent to the barrier edge. The positive (negative) value of Q_B is qualitatively similar to that associated with the $N^+N^-N^+$ structure; and there is a corresponding reduction (increase) in charge outside (inside) but adjacent to the barrier from that expected on the basis of classical calculations. Note: (i) the value of Q_B is approximately equal to the value of the self-consistent potential at the edges of the barrier; (ii) the density in the region of highest potential energy, is greater than the density in the center of the structure. (This variation in density is qualitatively accounted for by the value and sign of Q_B.) The inset to Fig. 2(e) is a combination of Q_B and potential energy plots. Figure 2(f) displays the energy per particle. The solid line is obtained from the Liouville equation and eqns (9a) and (9c). The dashed line is obtained from eqn (24) with the coefficient $a = 1/3$. The results are qualitatively in agreement, although the results adjacent to and outside of the barrier are in poor quantitative agreement. The energy per particle is dominated, as in the $N^+N^-N^+$ calculation by Q_B, and emphasizes the role of *gradients in the charge density* to the quantum contributions.

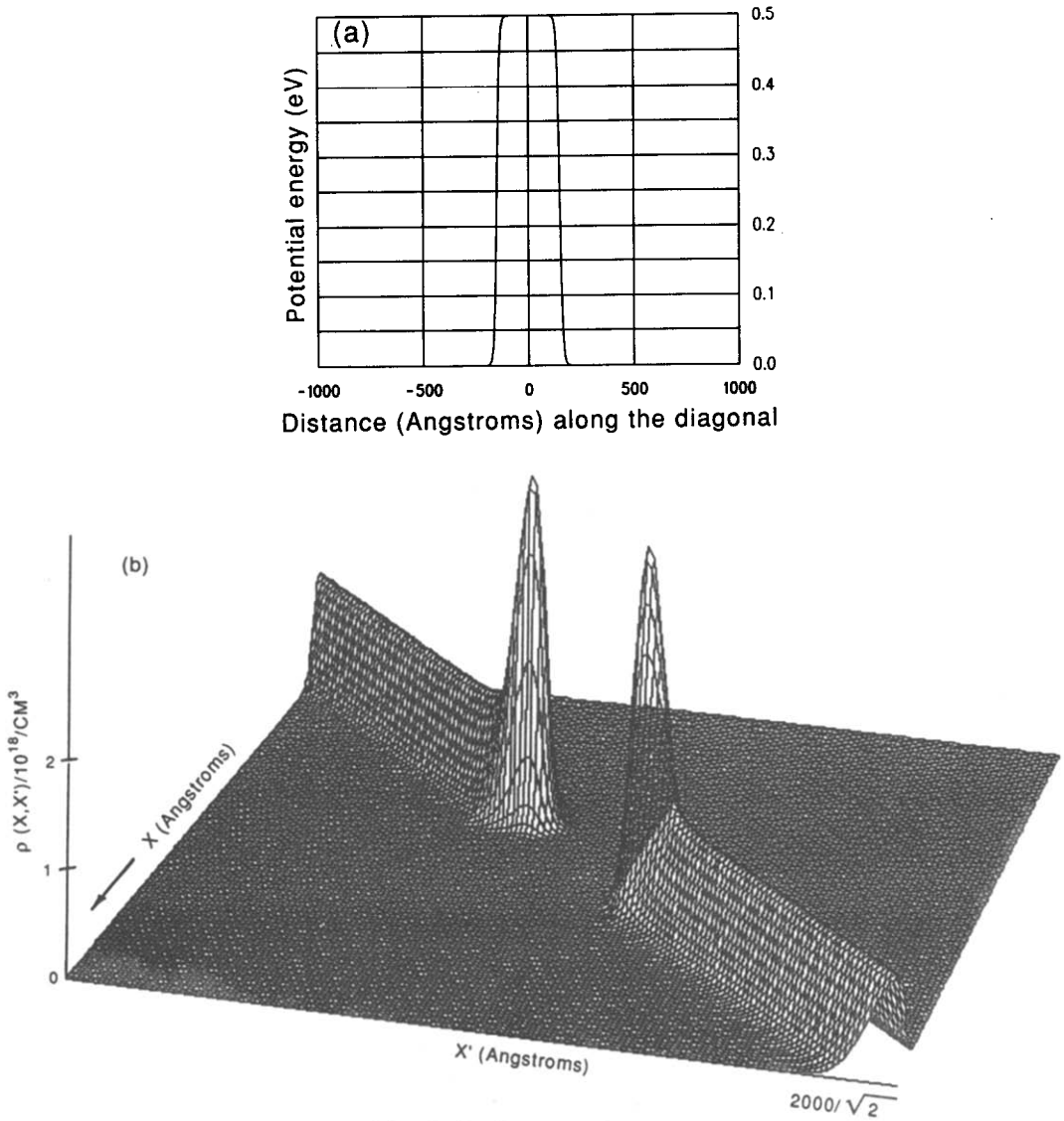

Fig. 2(a, b). *Caption on facing page.*

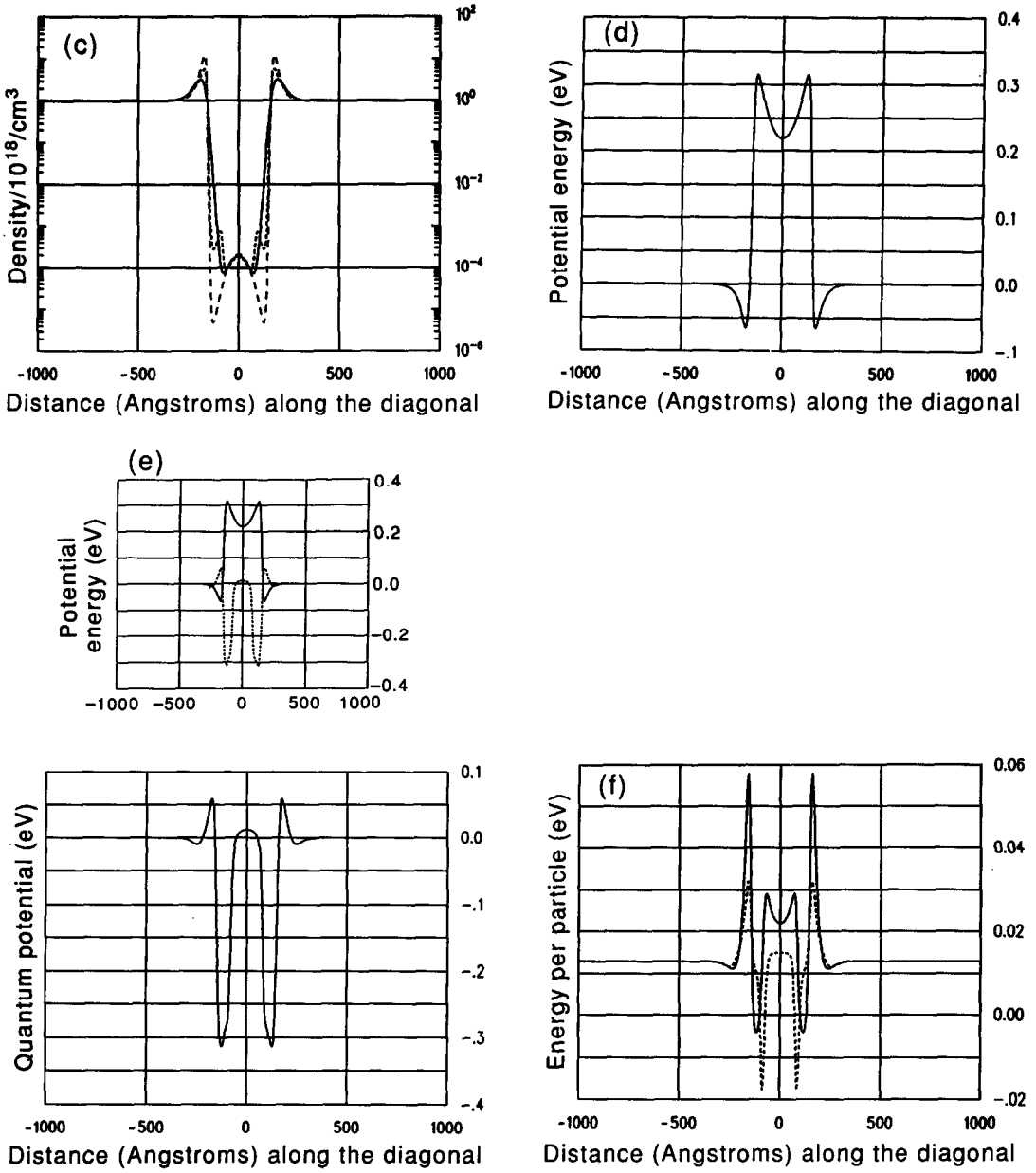

Fig. 2. (a) Sketch of the hyperbolic tangent barrier centrally placed within the 2000 Å structure. (b) Density matrix for the single barrier structure with free particle boundary conditions, as obtained from the Liouville equation (8). The physical dimension of the structure is 2000 Å, requiring that the density matrix, which is calculated over a square matrix, is of side $2000\ \text{Å}/\sqrt{2}$. The center of mass and nonlocal coordinates are indicated. (c) (——) Diagonal component of the density matrix from (a). (---) Density as obtained from eqn (4) with $a = 1/3$; (— —) with $a = 0$. (d) Self consistent potential energy for the calculation of (a). (e) Quantum potential for the calculation of (a). Inset includes (d). (f) (——) Energy per particle as obtained from eqn (9c). (---) Energy per particle as obtained from eqn (24) with $a = 1/3$.

THE APPROXIMATE NONEQUILIBRIUM DENSITY MATRIX; THE CONSTRUCTION OF THE QHD EQUATIONS

The nonequilibrium situation, is considered within the framework of the QHD equations, which incorporate quantum contributions as *modifications*. The QHD equations incude dissipation within the context of Fokker–Planck (FP) scattering. The motivation for FP dissipation is simplicity. When scattering is treated as in the Boltzmann transport equation, utilization of the Weyl transformation results in an equivalent scattering integral, that is approximately dependent upon powers of ζ, and derivatives with respect to ζ[10]. Under special circumstances these take the form of FP dissipation. The equation of

motion of the density matrix with FP dissipation[12] is:

$$\partial\rho/\partial t + (\hbar/2mi)(\nabla_x^2 - \nabla_{x'}^2)\rho - (1/i\hbar)[V(\mathbf{X}, t) - V(\mathbf{X}', t)]\rho + (1/2\tau)(\mathbf{X} - \mathbf{X}')\cdot(\nabla_x - \nabla_{x'})\rho + [(\Xi/\hbar^2)(X - X')\cdot(X - X')]\rho = 0, \quad (26)$$

where τ represents a scattering time, and Ξ represents a diffusive term in the momentum representation (see Appendix B). Using procedures leading to eqn (11), and assuming that the Ξ is directionally dependent, i.e. along the Y and Z, $\Xi = mk_b T/\tau$ (see also [7]), the equation from which the QHD equations are obtained is:

$$\partial\rho/\partial t + (\hbar/2mi)\partial^2\rho/\partial x\partial\zeta - (1/i\hbar)[2\zeta\partial V/\partial x + (\zeta^3/3) \times \partial^3 V/\partial x^3]\rho + (1/\tau)\zeta\partial\rho/\partial\zeta + (4\Xi/\hbar^2)\zeta^2\rho = 0. \quad (27)$$

We note that a general set of moment equations is obtained by taking successive nonlocal direction derivatives of the Liouville equation. Truncating the moment equations requires assumptions on the form of the density matrix; and that used below evolved from the approximate equilibrium case. The motivation for such a form is the semi-classical situation where moment equations are often trun-

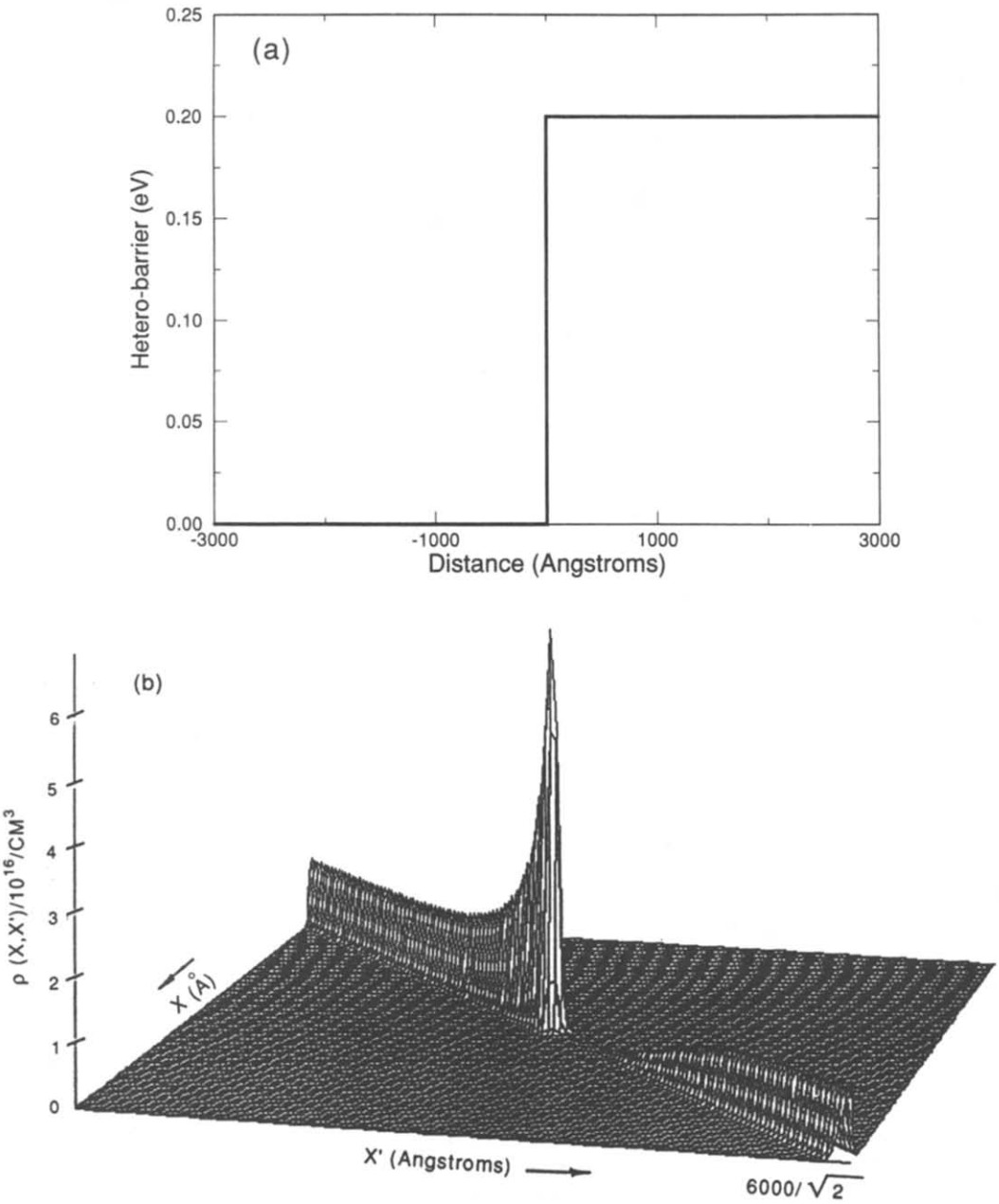

Fig. 3(a, b). *Caption on facing page.*

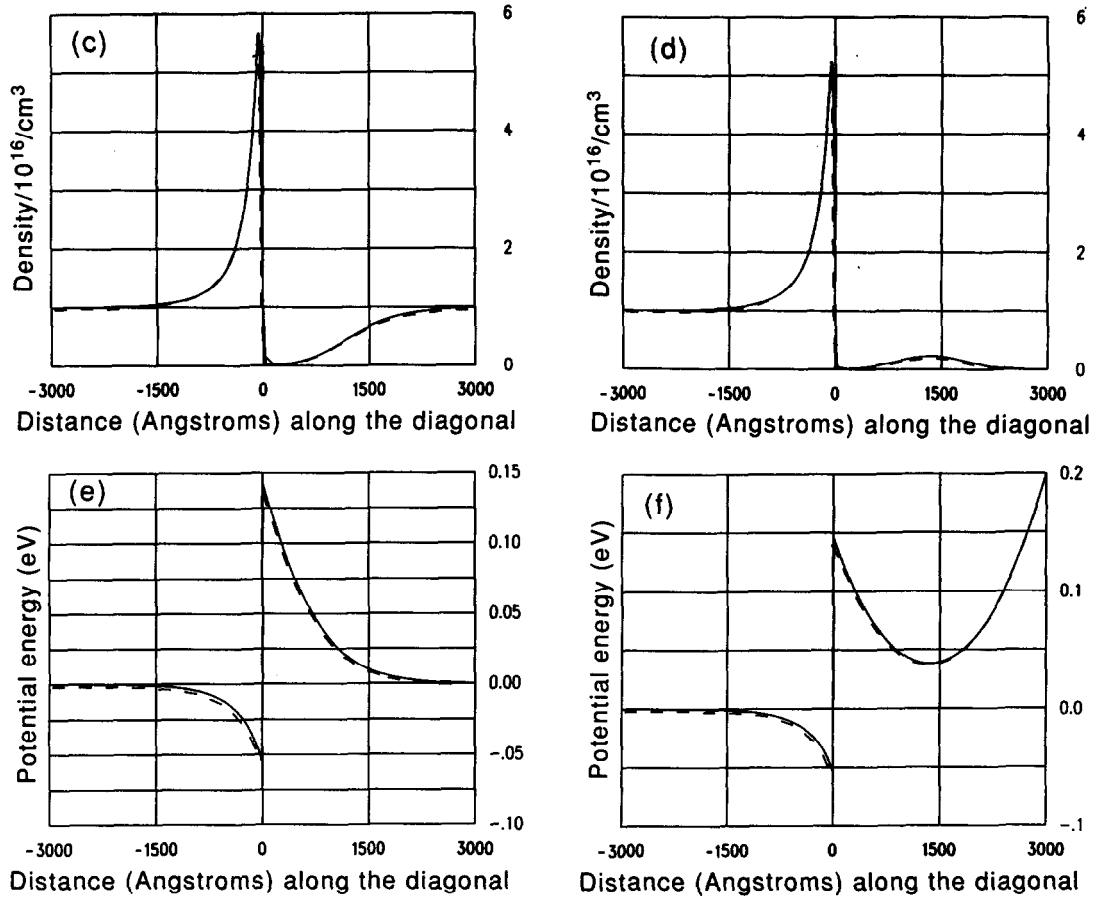

Fig. 3. (a) 200 meV barrier within the 6000 Å structure studied with the simulation. (b) Density matrix for the single barrier structure with free particle boundary conditions, as obtained from the Liouville equation (8) for a bias of −0.2 meV. The physical dimension of the structure is 6000 Å, requiring that the density matrix, which is calculated over a square matrix, is of side $6000\,\text{Å}/\sqrt{2}$. The center of mass and nonlocal coordinates are indicated. (c) (——) Self consistent diagonal component of the density matrix for a bias of −0.2 meV. (– – –) Quantum corrected solution. (d) (——) Self consistent diagonal component of the density matrix for a bias of 0.0 meV. (– – –) Quantum corrected solution. (e) (——) Self consistent potential energy for a bias of −0.2 meV. (– – –) Quantum corrected solution. (f) (——) Self consistent potential energy for a bias of 0.0 meV. (– – –) Quantum corrected solution.

cated by representing nonequilibrium by a displaced Maxwellian, $\exp-[\beta\{(p-p_d)^2/2m+V\}]$, and where the mean momentum, p_d, the density, and a particle temperature, are to be determined. The argument for a displaced Maxwellian is the assumption of rapid thermalization. While there is experimental evidence that some quantum feature size devices sustain strong relaxation effects, such phenomena is not likely to be universal. Nevertheless, as a first step in developing a set of nonequilibrium QHD equations we examine the consequences of modifying the quantum equilibrium distributions to describe nonequilibrium conditions. Within the context of the coordinate representation, the Weyl transformation as discussed in the Appendix B, dictates that the displaced equilibrium density matrix (generally non-Maxwellian) used below, is obtained through the following modification of a zero current density matrix:

$$\rho(x+\zeta, x-\zeta) \Rightarrow \rho(x+\zeta, x-\zeta)\exp+[2ip_d\zeta/\hbar], \quad (28)$$

where p_d is at most a function of x. With the current incorporated as in eqn (28) the *construction* of the QHD equations proceeds in three parts: *First*, the truncated density matrix is identified as eqn (28) with the form of the equilibrium contribution given by eqn (22) (the potential is replaced by the classical density equivalent); *second*, the relevant transport quantities are identified as carrier density, $\rho(x)$, mean momentum, $p_d(x)$ and electron temperature, $T_E(x) = 1/(\beta_E k_b)$; *third*, the moment equations, are obtained from a succession of derivatives, followed by the limit as $\zeta \Rightarrow 0$. In taking moments we note that much information contained in the off-diagonal elements of the density matrix is lost.

With eqn (28) the following quantities [from eqn (9)] are relevant to the moment equations (without the equipartition contributions of the Y and Z directions):

$$j(x,x) = \rho(x,x)p_d/m; \quad (29a)$$

$$E(x,x) = [p_d^2/2m + k_b T_E/2 - (\hbar^2/24m)\partial^2(\ln\rho)/\partial x^2]\rho; \quad (29b)$$

$$P^{(3)}(x,x) = [p_d^3 + 3p_d m k_b T_E - p_d(\hbar^2/4)\partial^2(\ln\rho)/\partial x^2]\rho. \quad (29c)$$

Equation (29c) is the diagonal component of $P^{(3)}(x+\zeta, x-\zeta) = (\hbar/2i)^3\partial^3\rho/\partial\zeta^3$, and represents the energy flux, (as typically appears, e.g. in the third moment of the Boltzmann transport equation). Equations (29) and their dependence on derivatives of density are valid only in the limits discussed in the above sections, and represent *modifications* to classical situations. *In this sense it is important to note that the derivation of the quantum potential in terms of* Q_W explicitly involved the carrier temperature. The Bohm potential Q_B, is independent of electron temperature. The consequences of using Q_B rather than Q_W, in the QHD equations should be examined.

The QHD equations are obtained by taking successive derivatives with respect to ζ, as defined by eqn (9) and taking the limit $\zeta \Rightarrow 0$. The *QHD particle, momentum and energy balance equations*, are respectively:

$$\partial\rho/\partial t + \partial[\rho p_d/m]/\partial x = 0; \quad (30)$$

$$\partial(\rho p_d)\partial t + 2\partial E(x,x)/\partial x + (\partial V/\partial x)\rho + \rho p_d/\tau = 0; \quad (31)$$

$$\partial E/\partial t + 1/(2m^2)\partial P^{(3)}/\partial x + (\rho p_d/m)\partial V/\partial x + 2E/\tau - (\Xi/m)\rho = 0. \quad (32)$$

We rearrange eqns (31) and (32), noting that the quantum correction driving force is *implicit* in $E(x,x)$ and $P^{(3)}(x,x)$. Using eqn (29b) for $E(x,x)$ and noting that $\partial[\rho\partial^2(\ln\rho)/\partial x^2]/\partial x = -(4m/\hbar^2)\rho\partial Q_B/\partial x$, the QHD momentum equation is[2]:

$$\partial(\rho p_d)/\partial t + \partial(\rho p_d^2/m)\partial x + \partial(\rho kT)/\partial x + \rho\partial(Q_B/3)/\partial x + \rho\partial V/\partial x + \rho p_d/\tau = 0, \quad (33)$$

which differs from its classical analog through the presence of Q_B[2]. When the first two terms are zero, and the electron temperature is spatially independent, the drift momentum density reduces to: $\rho p_d = -\tau k_b T\rho\partial[(V + Q_B/3)/k_b T + \ln(\rho)]/\partial x$. Then for $a = 1/3$: and $J = -e\rho p_d/m$, eqn (3) is retrieved; for $pd = 0$, the density, as given by eqn (4) is a solution to eqn (33). Note: the form of the scattering term in eqn (33) identifies the first part of the FP scattering as a frictional term (see [7]).

For the energy balance equation, using eqn (29), eqn (32) becomes:

$$\partial E/\partial t + \partial\{(p_d/m)[E + (\rho/\beta)(1 - [\lambda^2/6]\partial^2(\ln\rho)/\times\partial x^2)]\}/\partial x + (\rho p_d/m)V_x + 2E/\tau - (\Xi/m)\rho = 0. \quad (34)$$

To determine Ξ, we note that it generally depends upon x, as does τ. In the context of eqn (34) we require that E relax to E_0 which is the $p_d = 0$ value given by eqn (21). This is guaranteed with $\Xi = 2mE_0/\tau$. Thus eqn (34) becomes:

$$\partial E/\partial t + \partial[(p_d/m)(E + \rho k_b T)]\partial x + (\rho p_d/m)\partial[Q_B/3 + V]/\partial x - \rho(\lambda^2 k_b T/6)[\partial^2(\ln\rho)/\partial x^2]\partial \times (p_d/m)/\partial x + (2/\tau)[E - E_0] = 0. \quad (35)$$

The second part of the FP dissipation involves a relaxation to a non-zero thermal energy. E_0 above is the same as used by Woolard *et al.*[13].

The consequences of the above approximations is the appearance of the quantum potential with the factor "1/3". (The situation for Fermi statistics is not addressed here.)

QUANTUM MOMENT EQUATION COMPUTATIONS; COMPARISON TO THE EXACT SOLUTIONS

The development of the QHD equations, is predicted on future use in the design and understanding of multi-dimensional quantum feature size devices. The degree to which this is useful remains to be determined for nonequilibrium phenomena, and the work of [4,5] represents an important beginning. Another relevant case is the evaluation of density across an abrupt heterostructure region, as occurs in either a heterostructure diode or in modulation doped FETs. While the sheet charge density can be obtained from solutions to Schrodinger's equation, the incorporation of such a calculation in a quantum corrected standard set of device simulation equations has only recently been addressed. We consider this in assessing solutions of the QHD equations against the Liouville equation in the zero current limit. It is noted that the use of an abrupt interface violates the following conditions regarded as the basis for the development of the quantum modifications: *the potential is continuous, and the value of Q is small enough to be regarded as a "correction"*. It may be conjectured that the use of quantum potential has more generality than that uncovered in the above derivations; at this time there is no justification for this claim.

The computation is for a 6000 Å structure with constant $10^{16}/cm^3$ doping. The grid spacing for the Liouville equation was constant and equal to 7.5 Å; the grid was nonuniformly spaced for the QHD calculation. A 200 meV abrupt barrier is placed across the right half of the structure, as shown in Fig. 3(a). The self-consistent space charge profiles were computed for two values of applied bias: $V_{applied} = 0.0$ eV and -0.2 eV. In both computations the quantum potential was finite within the vicinity of the interface, with structure similar to that of the barrier problem discussed in Fig. 2; it was zero within the vicinity of the boundaries. The two dimensional zero current density matrix for $V_{applied} = -0.2$ eV is shown in Fig. 3(b).

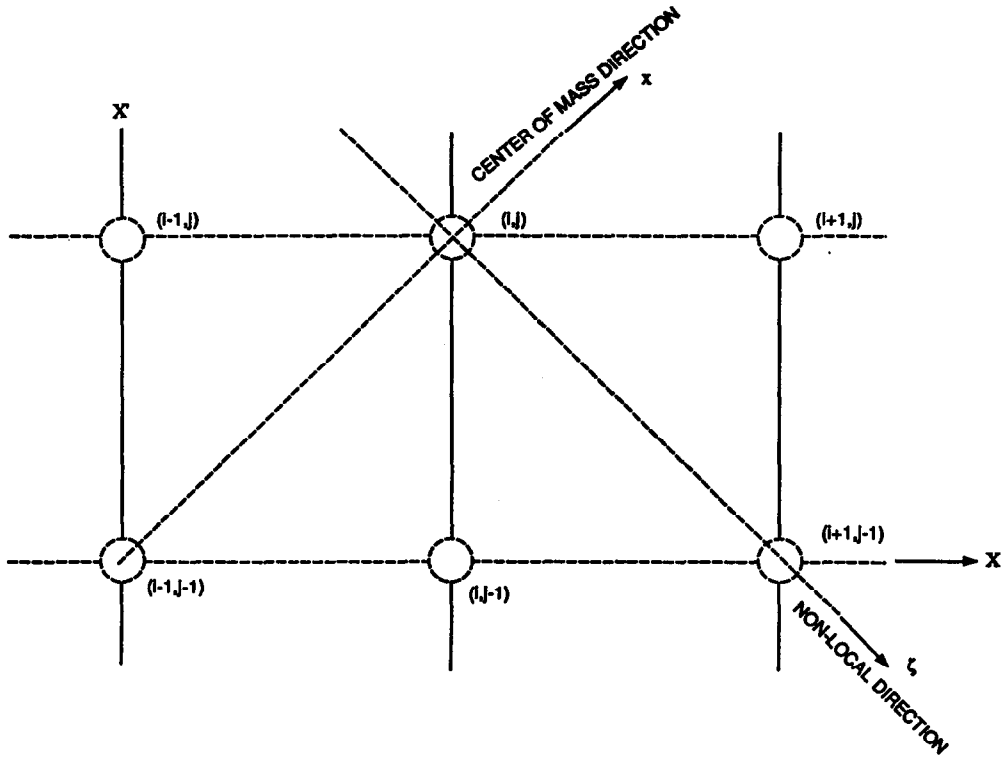

Fig. 4. Schematic representation of the characteristic directions with respect to the grid points.

Line plots of the density matrix for both the exact (solid line) and quantum corrected solution (dashed line) are displayed in Fig. 3(c,d). Note the accumulation of charge on the narrow bandgap side of the structure followed by depletion (with non-negligible values) of charge on the wide bandgap portion of the structure. Under bias the edge of the structure is depleted of charge. The potential energy distribution for the two values of bias are displayed in Fig. 3(e,f) where we see that the discontinuity in potential is equal to the full 200 meV associated with the barrier. The character of this solution is similar to that at the edge of the hyperbolic tangent barrier shown in Fig. 2. In particular the quantum potential is positive (negative) to the left (right) of the metallurgical boundary. The comparative density and potential profiles are extremely close and attest to the confidence of the approximation, for this type of structure. But caution is in order! The excellent agreement for the calculations of Fig. 3, *but* the less certain agreement of Fig. 2, indicate that a careful case-by-case assessement may be necessary. Nevertheless it appears that obtaining representative charge densities necessitates the incorporation of quantum effects through such additions as the Bohm quantum potential. Alternatively, realistic device simulations must resort to a full multidimensional quantum transport calculation.

SUMMARY

This study assessed the introduction of quantum modifications of classical transport, with the results indicating that quantum corrective transport is useful under certain circumstances, and that many simple device studies, such as those for HEMTs would benefit from its incorporation. It is likely that such corrective transport considerations would also be valuable under nonequilibrium conditions particularly in evaluating transport across heterostructure regions. It is important to note that introduction of the quantum potential in a generic form of the QHD equations is not new: it has been linked to density functional theory, as discussed by Deb and Ghosh[14] who also identify the force as being of quantum origin. Bohm and Hiley[15], point out that an essential new feature of the quantum potential is that for single particle Schrodinger fields, only the *form* of the Schrodinger field counts, not the intensity. The force arising from this potential is not like a mechanical force of a wave pushing on a particle with a pressure proportional to the wave intensity; rather the force arises from information content, e.g. structure, rather than value, of the wave[15]. Bohm and Hiley[15] distinguish this force from the Madelung[16] hydrodynamic model in which the particle is pushed mechanically by the fluid.

Acknowledgements—The authors are grateful for conversations with F. de Jong, G. J. Iafrate, W. Frensley, A. Kriman, M. Cahey, and especially D. K. Ferry. The authors are grateful for the assistance of B. Morrison. This work was supported by AFOSR, ARO and ONR.

REFERENCES

1. M. A. Ancona and G. J. Iafrate, *Phys. Rev. B* **39**, 9536 (1989).
2. H. L. Grubin and J. P. Kreskovsky, *Solid St. Electron.* **32**, 1071 (1989).
3. E. Wigner, *Phys. Rev.* **40**, 749 (1932).
4. J.-R. Zhou and D. K. Ferry, *IEEE Trans. Electron Devices* **39**, 1793 (1992).
5. J.-R. Zhou and D. K. Ferry, *Semicond. Sci. Technol* **7**, B546 (1992).
6. D. Bohm, *Phys. Rev.* **85**, 166, 180 (1952).
7. W. A. Frensley, *Rev. Mod. Phys.* **62**, 745 (1990).
8. G. J. Iafrate, H. L. Grubin and D. K. Ferry, *J. Physique* **C7**, 307 (1981).
9. H. L. Grubin, T. R. Govindan, B. J. Morrison, D. K. Ferry and M. A. Stroscio, *Semicond. Sci. Technol.* **7**, B360 (1992).
10. To be published.
11. A. M. Kriman, N. C. Kluksdahl and D. K. Ferry, *Phys. Rev. B* **36**, 5953 (1987).
12. A. O. Calderia and A. J. Leggett, *Physica* **A121**, 587 (1983).
13. D. L. Woolard, M. A. Stroscio, M. A. Littlejohn, R. J. Trew and H. L. Grubin, *Proc. Workshop on Computational Electronics*, p. 59. Kluwer Academic Publishers, Boston (1991).
14. B. M. Deb and S. K. Ghosh, *The Single-Particle Density in Physics and Chemistry*, p. 219. Academic Press, New York (1987).
15. D. Bohm and B. J. Hiley, *Foundations Phys.* **14**, 255 (1984).
16. E. Madelung, *Z. Phys* **40**, 332 (1926).
17. T. R. Govindan, H. L. Grubin and F. J. DeJong, *Proc. 1991 NASCODE.*
18. M. A. Stroscio, *Superlattices Microstruct.* **2**, 83 (1986).

APPENDIX A

Solution Procedure

For convenience of solution and determining suitable forms of boundary conditions, eqn (8), is rewritten as a coupled first order system of equations[17]:

$$u(X, X') + [i\hbar/2m][\partial\rho/\partial X + \partial\rho/\partial X'] = 0 \quad \text{(A1)}$$

$$\partial\rho/\partial t + [\partial u/\partial X - \partial u/\partial X'] + [i/\hbar][V(X, t) - V(X', t)]\rho = 0. \quad \text{(A2)}$$

Equation (A1) defines $u(X, X', t)$; eqn (A2) is an alternative form of eqn (8) after accounting for free particle conditions along the Y and Z directions; rewritten in terms of u and ρ. The characteristic directions for eqns (A1) and (A2) are:

$$x = (X + X')/2 = \text{constant} \quad \text{(A3)}$$

$$\zeta = (X - X')/2 = \text{constant}. \quad \text{(A4)}$$

In terms of the characteristic directions x and ζ, eqns (A1) and (A2) can be written as:

$$u(X, X') + [i\hbar/2m]\partial\rho/\partial x = 0 \quad \text{(A5)}$$

$$\partial\rho/\partial t + \partial u/\partial\zeta + [i/\hbar][V(X, t) - V(X', t)]\rho = 0. \quad \text{(A6)}$$

Suitable boundary conditions for eqns (A5) and (A6) are the specification of ρ and u along the boundary $X' = 0$ and the specification of u along the boundary $X = L/\sqrt{2}$, where L is the length of the device. Along the boundary $X = 0$, ρ is specified as the complex conjugate of $\rho(X, 0)$, since ρ is hermitian, and u is computed form the outgoing characteristic eqn (A6). Along the boundary $X = L/\sqrt{2}$, ρ is computed from the outgoing characteristic eqn (A5).

An alternative system can be formulated in terms of the current matrix:

$$j(X, X') + [i\hbar/2m]\partial\rho/\partial\zeta = 0 \quad \text{(A7)}$$

$$\partial\rho/\partial t + \partial j/\partial x + [i/\hbar][V(X, t) - V(X', t)]\rho = 0. \quad \text{(A8)}$$

Equations (A7) and (A8) have the same characteristic directions x and ζ as equations (A1) and (A2). Suitable boundary conditions for eqns (A7) and (A8) are the specification of ρ and j along the boundary $X' = 0$ and the specification of ρ along the boundary $X = L$. Along the boundary $X = 0$, j is specified as the complex conjugate of $j(x, 0)$ and ρ is computed from the outgoing characteristic eqn (A7). Along the boundary $X = L$, j is computed from the outgoing characteristic eqn (A8). Both sets of the first order system of equations, eqns (A5) and (A6) and eqns (A7) and (A8), are useful in applications since they allow different forms of boundary conditions. Both sets of equations can be solved by the same numerical procedure.

The solution procedure consists of solving the first order system of equations as an initial boundary-value problem starting from conditions along the line $X' = 0$ and marching to the line $X' = L$ using the method of characteristics. A characteristic net for the equation of motion of the density matrix can be constructed *a priori* from grid points of a uniform square grid. A discrete form of eqns (A5) and (A6) on this grid is [Fig. 4]:

$$[u]_{av} + [i\hbar/2m][\rho(i, j) - \rho(i-1, j-1)]/\Delta x = 0 \quad \text{(A9)}$$

$$[\partial\rho/\partial t]_{av} + [u(i+1, j-1) - u(i, j)]/\Delta\zeta + [i/\hbar][V(X, t) - V(X', t)]_{av}[\rho]_{av} = 0, \quad \text{(A10)}$$

where $[\cdot]_{av}$ represents an average over the grid cell. Depending upon the form of averaging chosen, eqns (A9) and (A10) form a system of 2×2 block tridiagonal or block diagonal algebraic equations that can be solved at $X' = j$ from known values at $X' = j - 1$. Thus, the solution procedure can be marched from boundary conditions at $X' = 0$, in steps along X', to $X' = L$. Similar procedures can be utilized for eqns (A7) and (A8).

Self-consistency is included in the analysis by iterating the solution of the density matrix equation with the solution of Poisson's equation to convergence, by successive substitution. For this purpose, Poisson's equation is written in the form:

$$\{\partial[\epsilon(x)\partial(\Delta V)/\partial x]/\partial x\}^n + e^2(\partial\rho/\partial V)\Delta V^n = -\{\partial[\epsilon(x)\partial V/\partial x]/\partial x\}^n - e^2[\rho(x, x) - \rho_0(x)]^n, \quad \text{(A11)}$$

with $V^{n+1} = V^n + \Delta V^n$, where n is the iteration number. The second term on the left hand side of equation (A11) serves to accelerate convergence of the iteration, wherein $\partial\rho/\partial V$ is evaluated at x either numerically from previous iterations or analytically as $\partial\rho/\partial V = -\rho(x, x)/k_b T$, for Boltzmann statistics. A 3-point centered finite difference approximation to (A11) results in a tridiagonal system of algebraic equations that can be solved easily and efficiently for ΔV, which is the increment in V between iterations.

The first step of the iteration procedure consists of assuming a distribution for the self consistent potential (typically, zero everywhere) and solving the density matrix equation to obtain the density distribution. Based on the computed density, Poisson's equation (A11) is solved to update the self consistent potential distribution. For the computations of this paper, the analytical expression for $\partial\rho/\partial V$ was utilized. For cases where $\partial\rho/\partial V$ is computed numerically, several iterations (typically, four or five) are required before a reliable estimate for the gradient can be computed. During these initial iterations, the second term in equation (A11) is replaced by a term of the form $-[\epsilon(x)\Delta V/(\Delta\tau\{\Delta x\}^2)]$ (Δx is the mesh spacing, $\Delta\tau \approx 50$) for

convergence. This term could be utilized for all iterations, but convergence is not rapid. Solution to Poisson's equation is used to update the self consistent potential based upon which the density matrix equation is solved again. The iterations are repeated until the density and potential distributions converge to the self consistent solution. For the computations presented here, six orders of residual reduction was obtained in less than 10 iterations.

APPENDIX B

Relation of Results to the Wigner Formulation

The connection between the density matrix in the coordinate representation and the Wigner function is through the Weyl-type transformations with normalizations peculiar to the problem of interest. For the density matrix:

$$\rho(\mathbf{x}+\zeta, \mathbf{x}-\zeta) = 2[1/(2\pi\hbar)]^3 \times \int_{-\infty}^{\infty} \mathrm{d}^3 p f_w(\mathbf{p}, \mathbf{x}) \exp[2i\mathbf{p}\cdot\zeta/\hbar], \quad \text{(B1)}$$

where the factor of 2 accounts for the fact that each momentum state can hold two electrons. The inverse transformation is:

$$f_w(\mathbf{p}, \mathbf{w}) = 2^3/2 \int_{-\infty}^{\infty} \mathrm{d}^3 \zeta \rho(\mathbf{x}+\zeta, \mathbf{x}-\zeta) \exp[-2i\mathbf{p}\cdot\zeta/\hbar], \quad \text{(B2)}$$

where the factor 2^3 is a consequence of the definition of the nonlocal coordinate [see eqn (7)]. In this transformation it is asserted that the Wigner function and all necessary derivatives with respect to momentum vanish as $p \Rightarrow \pm\infty$. Note: (a) $\rho(\mathbf{x}, \mathbf{x}) = [1/(2\pi\hbar)]^3 \int_{-\infty}^{\infty} \mathrm{d}^3 p f_w(\mathbf{p}, \mathbf{w})$; (b) substitution of eqn (12) into eqn (B2) yields the results: $f_w = \exp[-\beta\{(p^2/2m) + V(x) - E_F\}]$.

The Wigner equation including FP scattering, as discussed by Stroscio[18] is:

$$\partial f/\partial t + (p/m)\partial f/\partial x + (1/i\hbar)(1/2\pi\hbar) \int_{-\infty}^{+\infty} \mathrm{d}p' \int_{-\infty}^{+\infty} \mathrm{d}x' f(p', x) \times [V(x, t) - V(x', t)] \exp[i(p-p')x'/\hbar] = (1/\tau)\mathrm{div}_{\mathbf{p}}[\mathbf{p}f] + \Xi\nabla_{\mathbf{p}}^2 f, \quad \text{(B3)}$$

where, as in the main text, all spatial variations are along the x direction, Boltzmann statistics apply, and momentum variations in all three dimensions are allowed. The coefficients τ and Ξ are chosen as in the density matrix studies. For transport in one space dimension it is direct to demonstrate that the integral in eqn (B3) reduces in the classical case to $(\partial V/\partial x)(\partial f/\partial p)$. To second order in $\hbar$, the Wigner equation:

$$\partial f/\partial t + (p/m)\partial f/\partial x - \partial V/\partial x \partial f/\partial p + (\hbar^2/24)(\partial^3 V/\partial x^3)\partial^3 f/\partial p^3 = (1/\tau)\mathrm{div}_{\mathbf{p}}[\mathbf{p}f] + \Xi\nabla_{\mathbf{p}}^2 f. \quad \text{(B4)}$$

The left hand side of eqn (B2) has been discussed in [1,2]. Application of the transformation, eqn (B1), yields eqn (11).

In the absence of dissipation the approximate Wigner distribution function to second order in $\hbar$ is [Wigner[3], see, e.g. eqn (25)]:

$$f_w = \exp -\beta[p^2/2m + V(x)]\{1 - (\lambda^2\beta/4) \times [(\partial^2 V/\partial x^2 - \beta(\partial V/\partial x)^2/3) - \beta(p^2/3m)\partial^2 V/\partial x^2]\} \quad \text{(B5)}$$

which upon application of eqn (B1) yields the equation following eqn (22).

The relation between the density matrix and the Wigner function extends to observables, permitting a concise definition of the associated matrices. Defining *current density, energy density and third moment matricies* respectively, as:

$$\mathbf{j}(\mathbf{x}+\zeta, \mathbf{x}-\zeta) = 2[1/(2\pi\hbar)]^3 \times \int_{-\infty}^{\infty} \mathrm{d}^3 p(\mathbf{p}/m) f_w(\mathbf{p}, x) \exp[2i\mathbf{p}\cdot\zeta/\hbar] \quad \text{(B6)}$$

$$E(\mathbf{x}+\zeta, \mathbf{x}-\zeta) = 2[1/(2\pi\hbar)]^3 \times \int_{-\infty}^{\infty} \mathrm{d}^3 p(\mathbf{p}\cdot\mathbf{p}/2m) f_w(\mathbf{p}, \mathbf{x}) \exp[2i\mathbf{p}\cdot\zeta/\hbar] \quad \text{(B7)}$$

$$\mathbf{P}^{(3)}(\mathbf{x}+\zeta, \mathbf{x}-\zeta) = 2[1/(2\pi\hbar)]^3 \times \int_{-\infty}^{\infty} \mathrm{d}^3 p[\mathbf{p}(\mathbf{p}\cdot\mathbf{p})] f_w(\mathbf{p}, x) \exp[2i\mathbf{p}\cdot\zeta/\hbar], \quad \text{(B8)}$$

it is direct to demonstrate the validity of eqns (9b) and (9c). The derivative definition of the third moment [see discussion following eqn (29c)] follow directly from the above. Note: If the distribution function in eqn (B1) is for zero current, and a finite current function is obtained from $f_w(p - p_D, x)$, then the zero current and finite current density matrix are related as eqn (28).

APPENDIX C

Pure State Results and a Comparison to Iafrate, Grubin and Ferry[8]

The pure state results for current, energy density and third moment may be obtained as follows. Express the wave function as $\Psi(x, t) = \rho(x, t)^{1/2} \exp i\Theta(x, t)$, with $p(x, t) = \hbar\partial\Theta/\partial x$. Then Schrodinger's equation, $i\hbar\partial\Psi/\partial t = -(\hbar^2/2m)\partial^2\Psi/\partial x^2 + V(x, t)\Psi$, which is complex is rewritten as two real partial differential equations:

$$\partial\rho/\partial t + \partial j_{(\text{Schrodinger})}/\partial x = 0 \quad \text{(C1)}$$

$$\partial(\rho p)/\partial t + 2\partial E_{(\text{Schrodinger})}/\partial x + \rho\partial V/\partial x = 0, \quad \text{(C2)}$$

where

$$j_{(\text{Schrodinger})}(x, t) \equiv \rho(x, t)p/m \quad \text{(C3)}$$

$$E(x, t)_{(\text{Schrodinger})} \equiv [p^2/2m - (\hbar^2/8m)\partial^2(\ln\rho)/\partial x^2]\rho. \quad \text{(C4)}$$

While the content of Schrodinger's equation is contained in eqns (C1) and (C2), an expression for the time dependence of the energy may be obtained through the time derivative of eqn (C4) and judicious use of eqns (C1) and (C2). We find, with:

$$P^{(3)}_{(\text{Schrodinger})}(x, t) = [p^3 - (\hbar^2/4)\{3p\partial^2(\ln\rho)/\partial x^2 + \partial^2 p/\partial x^2\}]\rho \quad \text{(C5)}$$

$$\partial E_{\text{Schrodinger}}/\partial t + (1/2m^2)\partial P^{(3)}{}_{(\text{Schrodinger})}/\partial x + (\rho p/m)\partial V/\partial x = 0. \quad \text{(C6)}$$

Note the differences between the pure state definitions [eqns (C3), (C4), and (C5)], and that of eqns (29). For the pure state: *there is the absence of a temperature dependence, the factor of 3 is absent, and there is a velocity correction.*